DOI: 10.13009/EUCASS2019-608

DOI:

Assessment of the effect of heat-shield ablation on the aerodynamic performance of re-entry capsules in hypersonic flows

Alessandro Turchi[1†], *Sebastien Paris*[1], *Pasquale Walter Agostinelli*[1], *Felix Grigat*[2], *Stefan Löhle*[2], *Daniele Bianchi*[3], *and Luca Ferracina*[4]

[1]*von Karman Institute for Fluid Dynamics, Rhode-Saint-Genèse, Belgium*
[2]*University of Stuttgart, Institute of Space Systems, Stuttgart, Germany*
[3]*University of Rome "La Sapienza," Rome, Italy*
[4]*ATG Europe B.V. on behalf of ESA/ESTEC, Noordwijk, The Netherlands*

turchi@vki.ac.be · paris@vki.ac.be · agostinelli@vki.ac.be · fgrigat@irs.uni-stuttgart.de · loehle@irs.uni-stuttgart.de · daniele.bianchi@uniroma1.it · luca.ferracina@esa.int
[†]Corresponding author

Abstract

The recession of an ablative heat shield could significantly modify the nominal outer shape of a re-entry capsule and affect its aerodynamic behavior during the flight through the atmosphere. To quantify this effect, an experimental activity was carried out in the Mach-6 hypersonic wind tunnel H3 at the von Karman Institute for Fluid Dynamics. Subscale models of the European Space Agency hypervelocity entry demonstrator Phoebus, equipped with a heat shield made of a low-temperature ablator to promote the surface recession in the low-enthalpy conditions, were tested to record simultaneously the heat-shield recession and the aerodynamic loads. This paper describes the theoretical conception of this activity, details the preparation of the experimental test campaign and presents a first analysis of the experimental results.

1. Introduction

Ablative materials are used to build efficient Thermal Protection System (TPS) for planetary-entry capsules, as they represent the only practical solution to withstand the extreme heating conditions of high-speed entries and protect the underlying payload. An intrinsic drawback of these TPSs is that the material recession could induce the variation of the capsule's outer shape (technically referred to as the Outer Mold Line (OML)), hence modifying its aerodynamics.

Testing of thermal protection materials to study their response in relevant heating conditions is usually performed in plasma wind tunnels. However, if the goal is to understand how the ablation could influence the behavior of the full vehicle, the reproduction of the capsule aerodynamic is required, which is hardly possible in these kinds of facilities. Moreover, the chemically aggressive environment and the severe heat loads could significantly affect the accuracy of the force measurements that may be very sensitive to the temperature gradients. The aim of the present work is to shed some light on the OML shape-change influence on the aerodynamic behavior of entry vehicles by performing force measurements of a subscalescale ablative capsule under hypersonic conditions in the low-enthalpy flow of the von Karman Institute (VKI) H3 blow-down wind tunnel.

The design process of the subscale capsule, based on theoretical and numerical analyses to ensure a faithful reproduction of the extent of ablation of the full-size capsule in flight conditions, is explained first. Then, the test setup and the related measurement techniques to track the model recession and perform the force measurements are presented. Finally, the results of the test campaign, which includes testing at different angles of attack and total pressures, are shown and a first analysis of the influence of the shape change on the aerodynamic performance of the capsule is presented.

DOI: 10.13009/EUCASS2019-608

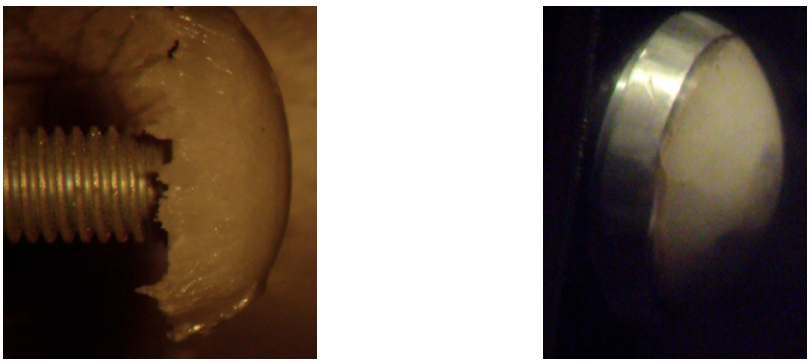

(a) Naphthalene model (b) Camphor model

Figure 1: Pictures of preliminary tests made on naphthalene and camphor in the H3 wind tunnel. Left: Solidification of molten naphthalene is evident in the aft part of the model, suggesting that pure sublimation is not achieved in the testing conditions. Right: The camphor model shows a significantly better behavior and no evidence of melting can be seen.

2. Ablative materials in low-enthalpy wind tunnels

The hypersonic wind tunnel selected for the the present study is the VKI H-3 facility. It is a Mach 6 blow-down tunnel able to provide a uniform axisymmetric jet 12-cm diameter and working with total pressures ranging from 6 bar to 35 bar. The test gas is heated up to a total temperature of 500 K in order to avoid condensation in the test section. The free-stream unit Reynolds number typically varies within 6 000 000/m-30 000 000/m.

Carbon-based ablative materials undergo a series of thermochemical processes including thermal decomposition (i.e., pyrolysis), heterogeneous reactions (e.g., oxidation), and sublimation. All these processes, which transform the carbonaceous material from solid to gas without undergoing melting, are triggered by the high-enthalpy flow and cannot be reproduced in a low-enthalpy facility ($T_0 \sim 500\,\mathrm{K}$) such as H3. Therefore, low-temperature ablators were considered and a trade off analysis was carried out to find a material that, under H3's testing conditions, could undergo an ablation process similar to the one experienced by real ablators.

Having in mind that the goal of the present study is the quantification of the effect that the shape change of the capsule's heat shield has on its aerodynamic behavior, reproducing the correct internal decomposition behavior (pyrolysis) of the heat shield was considered out of the scope. On the contrary, heterogeneous reactions and sublimation were considered of interest. Considering that as a rule of thumb it can be stated that oxidation is responsible for the heat shield ablation from low to mid heat-flux conditions, whereas sublimation is definitely the most important process in high heat-flux conditions, one can speculate that sublimation is the relevant phenomenon to be investigated when focusing on severe recession and shape change.

The mechanisms behind the sublimation process appears quite “simple" and reproducible in the considered test conditions. In fact, sublimation (i.e., direct transition between the solid and the gaseous state) is driven by the difference between the equilibrium vapor pressure of a given species and its actual vapor pressure next to the solid surface.[5] A change of material (i.e., change of equilibrium vapor pressure) would obviously affect the sublimation rate of the heat shield but, being the underlying physics driven by similar fundamental process, similarities for this ablation regimes between a flight and a low-enthalpy experiment may be found. For example, if one makes the simplified hypothesis that the surface temperature variation over the heat shield is negligible (i.e., the variation of vapor pressure with the temperature can be neglected), it can be imagined that the distribution of the sublimation rate over the heat shield follows the distribution of the heat-transfer coefficient, primarily affected by the pressure gradient over the surface, driven in turn by the shape of the capsule and the free-stream Mach number of the flow.

Naphthalene ($C_{10}H_8$) and camphor ($C_{10}H_{16}O$) were investigated as possible low-temperature ablators for the test-model heat shield. Camphor is characterized by a higher vapor pressure that naphthalene throughout the entire temperature range up to the melting point; hence, it sublimates at a higher rate than naphthalene when heated up to the same temperature. Moreover, camphor has higher triple-point pressure and temperature, therefore sublimating over a broader temperature range. This characteristic in particular is considered really advantageous since one of then main design constraints for the low-temperature heat shield is that melting has to be avoided. Preliminary tests revealed indeed a significantly different behavior of these two possible candidates when exposed to the Mach-6 jet in the H3 wind tunnel, with the naphthalene undergoing a mix of melting and sublimation and the camphor showing a much “cleaner” sublimation as clearly visible in Fig 1.

DOI: 10.13009/EUCASS2019-608

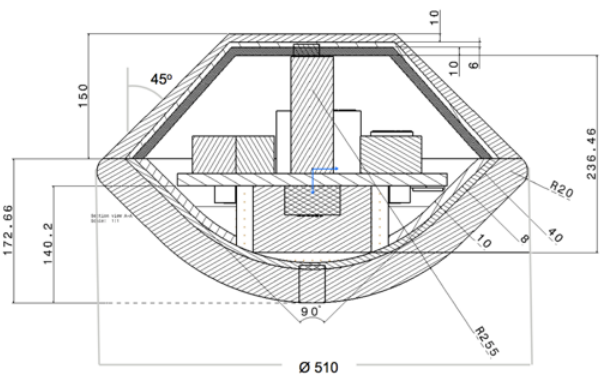

(a) Technical drawing of the Phoebus capsule[3]

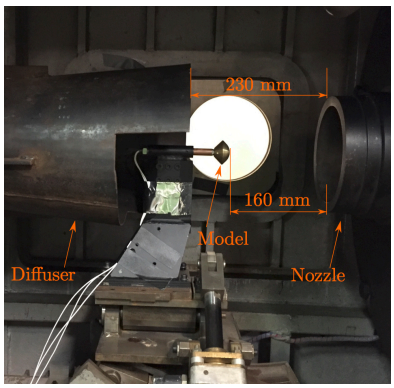

(b) Non-ablative (metal) 4-cm capsule installed into the H3 wind tunnel in the final testing configuration.

Figure 2: Full-size Phoebus capsule dimensions and subscale model installed in the H3 wind tunnel for testing.

3. Subscale ablative capsule design and manufacturing

Once identified the material to be used to make the low-temperature heat shield, the selection of the capsule of interest and the model design and manufacturing were carried out.

3.1 Capsule geometry selection and subscale model sizing

The Phoebus capsule,[3] Fig. 2a, was selected based on its relevance for the European Space Agency (ESA) and some preliminary numerical simulations that revealed as its shape (i.e., Hayabusa like) and size (i.e., 510 mm diameter) could make it severely prone to shape change during the re-entry. Phoebus has been designed to enter Earth's atmosphere at a speed of 11 km/s with an entry angle in the order of $-13.2°$. The mass of the capsule is approximately 25 kg and the OML is composed by a spherical nose up to 45° and a conical region. The TPS is used also at the shoulder of the vehicle that connects the front heat shield to the capsule aft body using a radius of curvature that is approximately 8% of the nose one.

The blockage effect is known to be a critical point in the hypersonic facilities. Therefore once the capsule shape was defined, the sizing of the subscale model to be tested required a dedicated analysis. The strategy that was followed for the definition of the model size tried to maximize its dimensions in order to simplify the following tasks (e.g., selection of an internal balance for the force measurements). Several Phoebus-like subscale capsules were produced and tested in the wind tunnel. 75-mm and a 60-mm capsules resulted in a total blockage of the tunnel. The 50-mm capsule was extensively tested by varying the distance from the nozzle exit and the diffuser position but every test resulted in a tunnel blockage. Finally, a 40-mm diameter capsule was successfully tested and this size was selected as the reference one for the design of the ablative capsules. Different relative positions of the capsule, the nozzle, and the diffuser were tested to find the best configuration shown in Fig. 2b.

3.2 Ablative capsule design and manufacturing

Different procedures to produce the ablative subscale Phoebus capsules have been tested during the activity. Based on the outcome of these preliminary attempts, also supported by literature data on similar activities on low-temperature ablators carried out in the past,[2,16] a procedure that relies on the sintering of deaerated camphor powder was selected as it proved to be the most reliable one in terms of model quality and repeatability. A sintering machine, which used the pressure applied through a 20-ton hydraulic press, was designed and built for the production of the test models. The sintering setup also included a vacuum pump employed to deaerate the camphor powder before applying the pressure load. The sintering procedure was then optimized by adjusting the possible parameters (e.g., vacuuming time, load time, powder mass, etc…).

The final subscale Phoebus models, shown in Fig. 3, were composed by a camphor heat shield (front part and shoulder exactly as in the full-size capsule, Fig. 2a) and a metal back cover, with the connection between the two being provided by the same metal interface that was mounted on the piston head and used to press the camphor into the mold. This interface was carefully designed to i) ensure that the camphor would stick to it after the sintering is finished; ii)

DOI: 10.13009/EUCASS2019-608

Figure 3: Good-quality subscale Phoebus model obtained using the final sintering procedure.

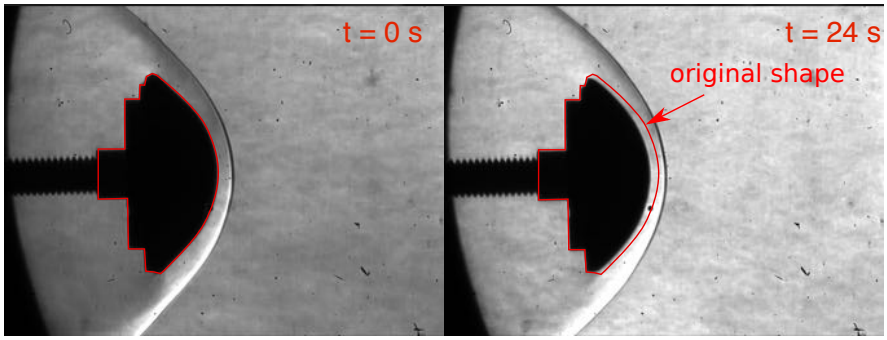

Figure 4: Schlieren images of a preliminary test performed on the front camphor heat shield in the H3 facility.

allow the excess powder to be evacuated during the sintering process; iii) provide an interface to house the internal balance inside the model (see section 4.1).

Preliminary tests performed on the subscale ablative capsules obtained by employing the described tools and procedures showed a satisfactory behavior of the heat shield. Figure 4 shows the Schlieren pictures of the initial and the final capsule configuration obtained during one of these preliminary tests performed on the front part of the capsule. The shape change of the camphor heat shield is visible from the Schlieren image after 24 s, where the nominal shape has been over imposed (red line).

4. Experimental setup

4.1 Force measurements

The Phoebus capsule is axisymmetric, hence no lateral aerodynamic loads are present and a plane of symmetry of the flow past the body always exists. Consequently, a 3-component balance was considered sufficient for the purpose of the present study. Given the reduced size of the model, a new balance that could fit inside the capsule back shell was designed and manufactured specifically for this test campaign. Typical test conditions of the H3 facility were used in the design phase of the balance along with the aerodynamic coefficients of a standard capsule (i.e., Apollo Command Module).

After the balance design, the stress expected on the balance during a typical H3 test were checked numerically through a finite element analysis to find the best positioning of the strain gages. This ensured that a non-negligible stress could be generated at the location of the single-component strain gages when a pure (unidirectional) load is applied in the corresponding direction. After, in order to check the validity of the balance design and the optimal location of the strain gages, a numerical calibration was performed. It consisted in the application of pure loads (i.e., axial force, normal force and pitching moment) and the computation of the stress at the identified strain-gage positions to build a theoretical transfer function that could be used to rebuild the different force components when a combined numerical load was applied. Comparison of the computed components with the prescribed values allowed verification of the balance design and the strain-gage optimal positioning. Figure 5a shows the assembly of the designed balance, the interface for the camphor heat shield installation and the back cover of the capsule.

The manufacturing of the balance was performed using electrical discharge machining to reduce the residual internal stress, the balance before instrumentation is shown in Fig. 5b. The instrumentation of the balance, consisting

DOI: 10.13009/EUCASS2019-608

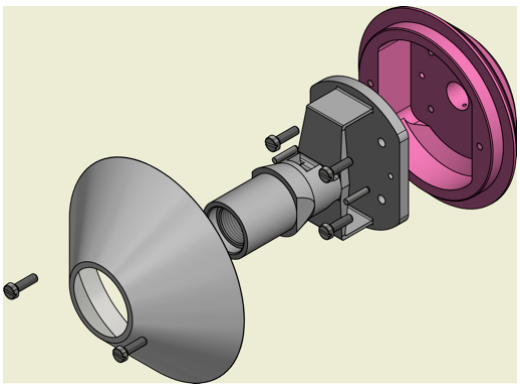

(a) Subscale capsule assembly.

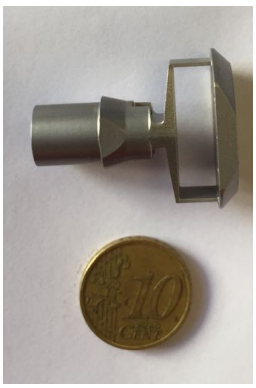

(b) 3-component balance before installation of the strain gages.

Figure 5: Left: CAD drawing of the assembly of the ablative capsule composed by the interface, the balance and the back cover (ablative heat shield is not shown); Right: 3-component balance after manufacturing.

in positioning strain gages at the identified locations, was done by the Fine-Mechanics Lab of the VKI Workshop. The actual calibration of the balance was performed using the calibration bench available at the VKI. The balance was placed inside an interface that allows to apply loads at precise locations in order to produce pure (axial or normal) forces and pitching moment or combinations of these loads. This calibration step allowed to build the final calibration matrix for the new balance.

4.2 Recession measurements

Two different types of recession measurement were included in the experimental setup.

4.2.1 Photogrammetry

Photogrammetry has long been used for calculating 3D geometries on the basis of 2D imaging.[11] The photogrammetry techniques were developed primarily for mapping large scale regions, e.g. generating landscape topography or generating 3D models of buildings. Close range photogrammetry, that is the study of millimeter or smaller scale objects is a more recent application of the same techniques. Recession measurements performed by means of photogrammetry, as demonstrated by Schairer and Heineck,[15] Löhle[9,10] and Reimer,[13,14] can potentially achieve the most accurate results. In principle the only limitation is the resolution of the employed cameras, and using modern cameras spatial resolutions in the order of micrometers can be achieved.

The photogrammetry measurements in the H3 facility were performed using a system developed at Institut für Raumfahrtsysteme (IRS), which was installed at VKI. However, some adaptations were necessary due to the geometrical constraints related to the optical access to the test section and the relatively short distance between the test article and the nozzle exit. In particular, two front coated mirrors were installed on the facility wall upstream of the nozzle to allow a satisfactory view angle of 68°-71° between the cameras, i.e. the angle between the two optical axes, through the reflected paths. A CAD design of the IRS photogrammetry setup adapted to the H3 facility is shown in Fig. 6a. Two Canon EOS 5D SR cameras with 50 Mpx sensors, each with a 1200-mm focal length (zoom lens of 600 mm focal length plus additional 2x-teleconverters), were used in this setup.

The *drawback* for a useful photogrammetric data analysis is the requirement of sufficient visible structures on the surface to be analyzed. For standard ablator performance analysis this is the surface of the ablator itself. However, the surface of sintered camphor is semi transparent (see Fig. 3), therefore a further development of this very accurate and unique ablation recession measurement method was necessary. Different approaches were analyzed prior to the official test campaign in order to project structures to the camphor surface which in turn can be acquired by the photogrammetric measurement system. Finally, the projection of concentric circles on the sample surface was selected as the most promising approach and tests with different optical setups were analyzed, by varying the mirror and camera positions as well as the camera settings. A picture of the ablative sample before testing, with the circular pattern clearly visible on it, is shown in Fig. 6b.

It was originally assumed that the projector light would mainly be reflected from the camphor surface as shown in Fig. 6b. However, the analysis of the data showed clearly that the camphor became practically transparent only

DOI: 10.13009/EUCASS2019-608

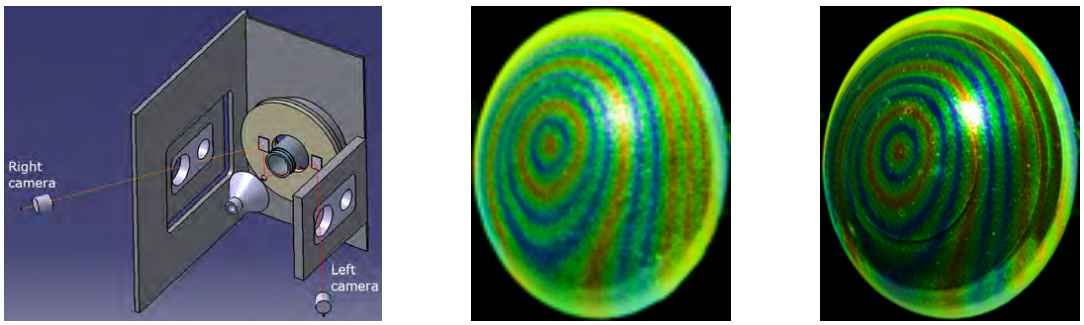

(a) CAD model of the camera setup. (b) Patterns before testing. (c) Patterns during testing.

Figure 6: Camera positioning and circular patterns projection on the camphor model (before and during testing) for the photogrammetric measurements.

few seconds after the model injection. The projected pattern is mostly reflected from the underlying metal interface on which the ablative heat shield was attached (Fig. 6c). Therefore the surface originally recovered through the photogrammetry only represented a refracted 3-D model of the metal surface. The solution for this issue is the calculation of the refraction in order to estimate the actual position of the camphor surface. This model uses the fact that the refraction changes as the thickness of the camphor layer decreases.

4.2.2 Side-on measurements

Side-on profile tracking was considered as an additional non-intrusive technique to be used in parallel to the photogrammetry setup. Measurements of this nature are the current baseline for various plasma facilities where ablation testing is performed.[6,7,12] Fine surface details cannot be retrieved with this technique but, in turn, the time evolution of the test article can be obtained with a simple analysis of the recorded video assuming that the heat shield evolution does not affects the axial symmetry of the sample. In the present analysis, the relatively simple setup necessary to implement this technique represented an additional advantage as it could be used in parallel to the photogrammetry without interfering with its more complex setup. The side-on measurement setup was put in place using a standard Nikon D5000 camera. The camera was operated in video mode (24 fps), which allows an approximate resolution of 0.9 MP. Using a 200-mm focal length the final achieved spatial resolution was, in average for all the performed test, ± 0.140 mm.

5. Flight relevance of H3 testing and final test matrix definition

The capability of the H3 facility acted, as a matter of fact, as the main constraints in the definition of the testing conditions. However, an analysis of the representativeness of these conditions for the Phoebus capsule under investigation was deemed necessary. This analysis was carried out considering that the goal of the H3 test campaign was to observe the variation of the aerodynamic forces on the capsule when its outer shape is modified by ablation. Therefore, a full duplication of the flight conditions was not in the scope. On the contrary, the correct duplication of the ablated profile is of primary importance. As discussed earlier, the sublimation regime of ablation is definitely the more severe in terms of recession. For this reason, the ablation experienced at the peak-heating point along the trajectory was considered relevant for the present study.

A first theoretical dimensional analysis aimed to compare the expected recession of the camphor heat shield (subscale model) in the H3 facility to the recession experienced by a real carbon-phenolic heat shield (fullscale capsule) during the Phoebus entry. This analysis revealed that the H3 testing could be fully relevant in terms of relative variation of TPS thickness if the first few seconds of the test run are considered. This was recognized as favorable outcome for both the present and the following activities which consist of the evaluation of the effect of ablation on the static aerodynamic behavior of the capsule in hypersonic conditions, and the analysis of the stability behavior of the ablated capsule in transonic regime, respectively. In addition, since what concerns the shape change is the distribution of the recession along the heat shield, it is important to remark that i) the ablation distribution follows closely the heat flux distribution; ii) according to Lees,[8] the heat flux distribution over a spherical nose is insensitive to the Mach number (i.e., a similar distribution is expected for the $M = 28$ of the flight and the $M = 6$ of the test); and iii) the heat flux distribution over of the conical part of a sphere-cone object is mainly driven by the cone half angle, which is the same

DOI: 10.13009/EUCASS2019-608

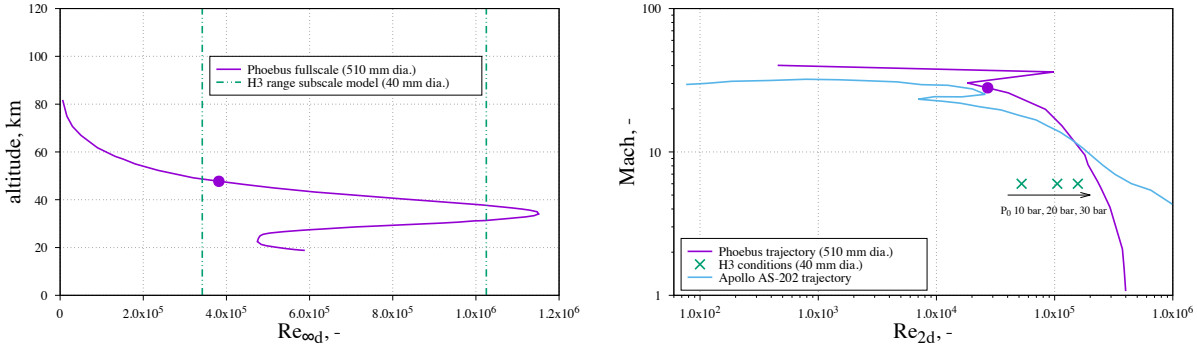

(a) Free-stream Reynolds number.

(b) Post-shock Reynolds number.

Figure 7: Left: Comparison between the free-stream Reynolds-number range achievable in the H3 facility for the subscale capsule and the expected Reynolds numbers along the fullscale Phoebus trajectory; Right: Post-shock Reynolds number versus Mach number for the Phoebus trajectory and for the H3 facility. Apollo data from mission[4] are shown for comparison. The peak of convective heat flux for Phoebus is marked with a dot.

for the real capsule and the model.[8] Therefore, the shape change experienced by the camphor model tested at Mach 6 in the H3 wind tunnel should be totally representative of the shape change that the real capsule would undergo along its trajectory.

The duplication of the free-stream Reynolds number was also considered of possible interest. A comparison of the Reynolds numbers achievable in the H3 facility with the expected values along the Phoebus trajectory is given in Fig. 7a. Interestingly, the majority of the Reynolds (the reference lengths are the fullscale and subscale capsule diameters for the flight and the test, respectively) covered along the trajectory after the peak heating (marked with a dot in Fig. 7a) can be reproduced in the facility. In particular, testing at a low total pressure ($\sim$ 10 MPa), would allow to reproduce pretty well the free-stream Reynolds number at the trajectory peak-heating point.

As reported by Griffith[4] a more pertinent similarity parameter when dealing with the experimental reproduction of flows about very blunt bodies is the shock Reynolds number $\mathrm{Re}_{2\mathrm{d}}$, i.e., the Reynolds number calculated using the post-shock conditions and the capsule diameter. In particular, considering that our interest lies within the study of the aerodynamic coefficients of the Phoebus capsule, their dependency on $\mathrm{Re}_{2\mathrm{d}}$ need to be clarified in order to ensure testing in relevant conditions. Figure 7b presents the $\mathrm{Re}_{2\mathrm{d}}$ evolution with the Mach number for the trajectory of Phoebus along with the expected values of $\mathrm{Re}_{2\mathrm{d}}$ for three different total pressure levels in the VKI H3 facility. Data from Apollo mission AS-202 given by Griffith[4] are also shown for comparison. As seen, the H3 $\mathrm{Re}_{2\mathrm{d}}$ values could cover a substantial part of the Phoebus trajectory below the peak heating (marked with a diamond symbol at Mach 28), therefore the wind tunnel tests can be considered representative.

Based on the above arguments, the final test matrix for the ablative models was defined to span three different total pressures and three different angles of attack (AoAs) for a total of nine tests. The testing conditions are summarized in Table 1.

Table 1: H3 test conditions for the subscale ablative Phoebus capsule.

AoA	Test no.	M	p_0 [Pa]	$\mathrm{Re}_{\infty\mathrm{d}}$	$\mathrm{Re}_{2\mathrm{d}}$ (perfect gas)	$\mathrm{Re}_{2\mathrm{d}}$ (real gas)
0°	1	6.00	2.50×10^6	8.55×10^5	1.27×10^5	1.32×10^5
	2	6.00	2.00×10^6	6.84×10^5	1.02×10^5	1.06×10^5
	3	6.00	1.50×10^6	5.13×10^5	7.65×10^4	7.92×10^4
2°	4	6.00	2.50×10^6	8.55×10^5	1.27×10^5	1.32×10^5
	5	6.00	2.00×10^6	6.84×10^5	1.02×10^5	1.06×10^5
	6	6.00	1.50×10^6	5.13×10^5	7.65×10^4	7.92×10^4
4°	7	6.00	2.50×10^6	8.55×10^5	1.27×10^5	1.32×10^5
	8	6.00	2.00×10^6	6.84×10^5	1.02×10^5	1.06×10^5
	9	6.00	1.50×10^6	5.13×10^5	7.65×10^4	7.92×10^4

DOI: 10.13009/EUCASS2019-608

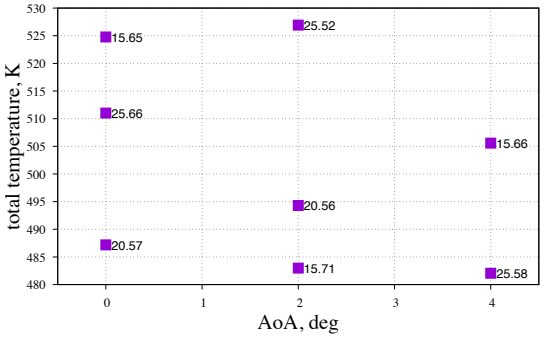

(a) Total temperature vs AoA with total pressure as parameter.

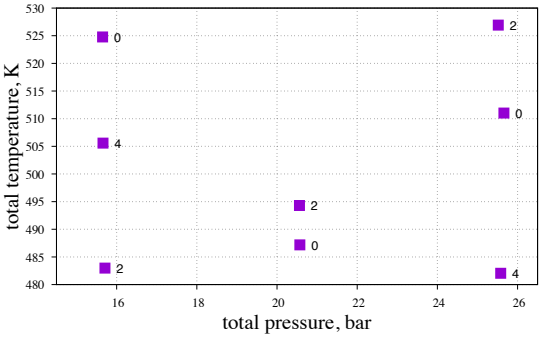

(b) Total temperature vs total pressure with AoA as parameter.

Figure 8: Average actual total quantities measured during the nine ablative tests of Table 1. Temperature data for test no. 8 are not given due to a malfunctioning of the acquisition system.

6. Results and discussion

The test matrix given in Table 1 was covered within a full week of testing. Each model was manufactured, following the established sintering procedure, right before each test to reduce as much as possible the premature recession of the camphor heat shield. The nominal conditions listed in Table 1 were satisfactory achieved for all the nine tests as shown in Fig. 8, where the time-averaged measured total pressures and total temperatures are given. Note that due to a malfunctioning of the acquisition system the temperature of test no. 8 was not recorded.

Figure 9 shows a typical output (test no. 1) of the side-on recession measurement and gives an indication of the extent of shape change experienced by the test samples. Several typical features of the ablative tests are visible in these images. First, as anticipated in section 4.2.1, the quality of the surface of the camphor changes during the test and the projected ring become more evident as they are being reflected by the underlying metal interface. Some cracks were detected for the majority of the tests, yet in the most of the cases they did not represent an issue as it was verified, by analyzing the high-resolution images of the photogrammetry system, that they were mostly internal and did not compromise the quality of the test sample. However, for few cases, the failure of the heat shield caused by some local weaknesses marked the premature end of the relevant part of the test. Cracks in the camphor are visible in Fig. 9c. The comparison of Figs. 9a-9c also revealed that the corner of the heat shield (i.e., the *shoulder*) was typically flattened quite fast during the the test. This typical response of the test samples have the main disadvantage of exposing the sharp corner of the metal back shell directly to the flow with obvious consequences on the capsule aerodynamics. However, it has to be noted that the ablation experienced in a pure sublimation regime, as the one occurring for the camphor heat shield, is significantly affected by the local pressure. Consequently, the high recession of the shoulder is driven by the significant drop in wall pressure in that region. Therefore, considering that the ablation of a real TPS is the result of the the interplay of different thermochemical processes (e.g., oxidation and sublimation), which might be not so strongly dependent on the local static pressure, drawing direct conclusions on the behavior of the shoulder in the fullscale case from these tests might be misleading. Indeed, a parallel numerical activity, which goes beyond the scope

Table 2: Time occurrence of the identified failure modes.

	Time of appearance [s]	
Test no.	**Metal edge**	**Dent**
1	12	-
2	7	21
3	4	22
4	12	-
5	20	-
6	-	19
7	17	-
8	3	14
9	4	15

DOI: 10.13009/EUCASS2019-608

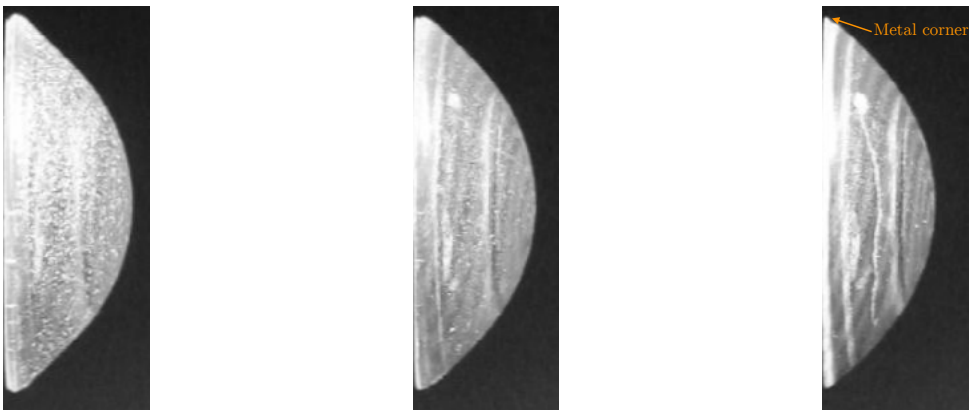

(a) 0 s. (b) 8 s. (c) 19 s.

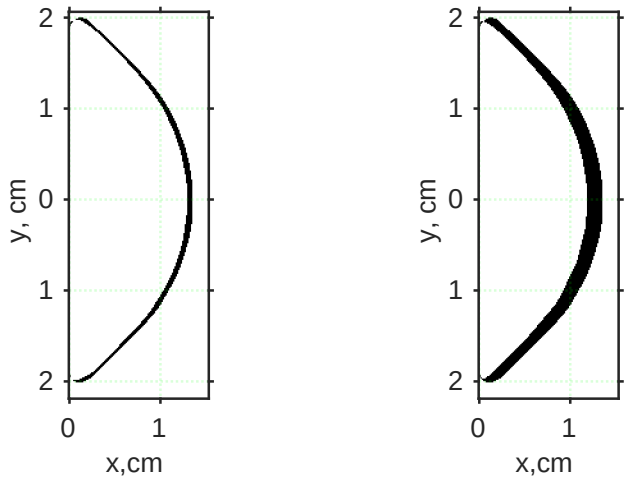

(d) Shape change at 8 s. (e) Shape change at 19 s.

Figure 9: Side-on views at 0 s (a) and 8 s (b) and 19 s (c) during test no. 1. The shape change obtained after post-processing of these images is given in (d) and (c) for 8 s and 19 s, respectively, where the ablated part of the heat shield is represented in black.

of the present paper, was undertaken to steer the analysis of the test data and their relevance for the real mission. This analysis is presented in a companion work.[1]

Overall, the nine tests were performed successfully with no major failures of the setup. Considering that the deterioration of the heat shield integrity could jeopardize the analysis of the test data, the high-resolution images from the photogrammetry system were analyzed to detect the appearance of those event identified as “failure modes" (Table 2). Generally, the higher the pressure the more demanding the test appeared to be for the camphor. Consequently the tests performed at high pressure were often affected by the appearance of a non-negligible defect on the heat shield. In the case of good performance of the heat shield throughout the whole test, the exposure of the metal edge of the back cover to the flow (see Fig. 9c) represented a major event to be taken into consideration during the analysis of the results.

6.1 Recession and shape change

Both recession measurements were performed in each test. Due to all the important limitations caused by the aspect of the camphor, already mentioned in section 4.2.1, and the additional geometrical constraints caused by short distance between the model and the nozzle exit, accurate photogrammetric data could be obtained exclusively for a central region of the heat shield (see Fig. 10), with a decreasing resolution towards the shoulder. In general, the center-line recessions estimated by the two different measurement techniques were found to be in satisfactory agreement between each other. This was considered as a validation for the side-on measurements that, considering the invariance of the resolution along the heat shield, have been used for the evaluation of the shape change (see Fig. 9e).

DOI: 10.13009/EUCASS2019-608

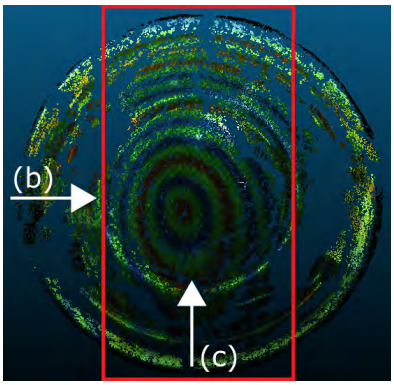

(a) Front view.

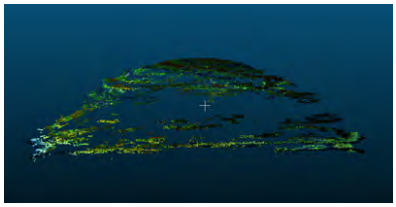

(b) Side view.

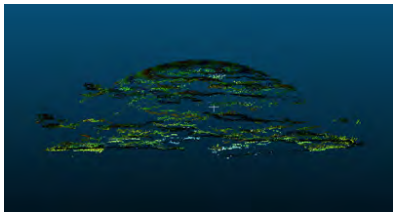

(c) Bottom view.

Figure 10: Photogrammetry point clouds from different views for test no. 5. The region within which the surface could be accurately reconstructed and used for further analysis is marked in (a).

Figure 11a shows the parabolic fitting (found to be the most accurate) of the center-line recession for all the tests. This figure considers the whole test time and the y axis has been limited to the known camphor thickness in that region (~ 2.20 mm) plus the estimated accuracy of the side-on measurements (~ 0.200 mm). The plot uses the colors to discern the different test pressures and the line-dash style to indicate the AoA. The same convention will be used for any plot throughout this paper. From the curves it can be seen that the center-line recession almost always hit the bottom of the heat shield, with test no. 4 (lowest pressure and temperature, see Fig. 8) representing an exception. Tests at the same pressure are obviously related and the extent of recession varies because of the difference in total temperature. When total temperatures are neatly separated, e.g., tests no. 1, 4, and 7 or tests 3, 6 and 9, the center-line recession seems to increase with the increasing temperature. However, when the total temperatures are close enough, i.e., tests no. 2 and 5, the fact that the centerline does not correspond to the stagnation line when an AoA is present seems to influence the relative order of the recession (maximum at the stagnation point). Test no. 8, for which the test total temperature was not recorded, presents an unusual recession curve. Moreover, the post processing of it after approximatively 17 s of test could not be performed due to a major failure of the test sample that could be also confirmed from the balance data as it will be shown later on. Figure 11b presents the recession data limited to the “relevant test time," identified as the time before the first of the two failure modes was detected. In this case, a linear fitting of these subset of data is shown in logarithmic scale.

Due to the limited range of the analyzed AoAs, the shape change appeared to be minimally affected by the capsule orientation, with small asymmetries between the upper and the lower part of the heat shield that could be detected only by the photogrammetry. The recession of the stagnation region appears to be more important than the recession in the conical part of the heat shield causing a non negligible shape change. The ratio between the maximum diameter of the capsule (at its shoulder) and the distance along the centerline from the surface to the plane where the maximum diameter is located was considered a relevant parameter to check. Interestingly, the non-negligible recession rate experienced by the shoulder within the first seconds of testing results in a small variation of this ratio, that instead decreases drastically once the shoulder is significantly ablated and the frontal area does not decrease anymore due to the presence of the metal back cover.

DOI: 10.13009/EUCASS2019-608

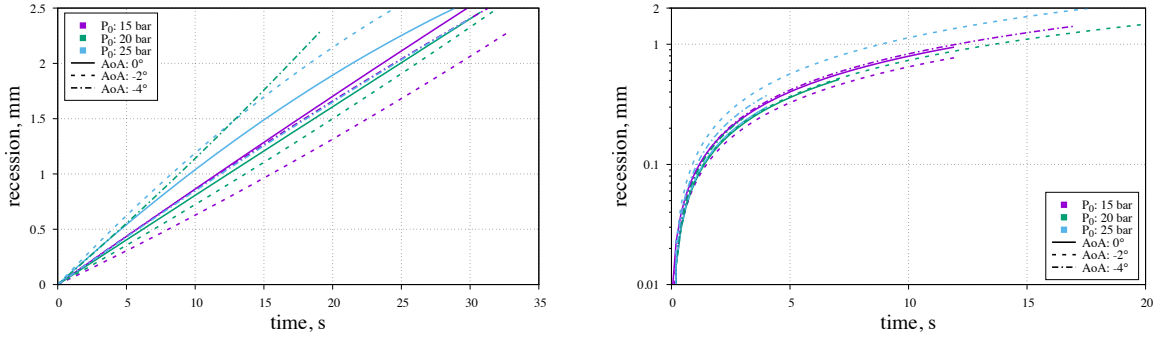

(a) Parabolic fitting of the whole test duration.

(b) Linear fitting of the “relevant phase" of the test, i.e., before the first of the two possible failures compromises the heat shield.

Figure 11: Fitting of center-line recession measurements obtained from the side-on tracking (average accuracy of measurement ±0.140 mm).

6.2 Aerodynamic coefficients

The same procedure was followed for each test run. First, the internal balance was installed in the ablative model, the sample was mounted on the support inside the test chamber and aligned. Then all the balance components nullified with the capsule in its final position, the model retracted, the signal recording activated and the tunnel started. Finally, once the flow was established and the testing conditions met, the capsule was injected into the stream and the test started. After the test, the three recorded components of the balance were then postprocessed using the calibration matrix and the measured test conditions to extract the aerodynamic coefficients of the subscale capsule and their variation.

A summary of the obtained aerodynamic coefficients and their evolution during the full test is given in Fig. 12. The nominal surface area and diameter of the subscale capsule were used for the determination of these coefficients for the whole test duration. Two out of the three tests at 25 bar experienced a partial balance malfunctioning and part of the data are not available. For test no. 3 few measurement points are available at injection, but it is only at 15 s that the balance started recording steadily. However, the entry-point value for the z component seems to be not in line with the data from all the other tests at the same pressure. For test no. 6 the entry value is missing and the balance worked only intermittently before 13 s, after that a steady recording is achieved. only at around 15 s the balance In general, from the balance data it is possible to detect when a dent is formed on the heat shield. Depending on the location of the heat shield failure, at least one of the three balance component seems to record an abrupt slope variation at a time that is compatible with those given in Table 2.

A first consideration on the quantitative behavior of the balance components relates to the magnitude of the measured forces and moment. In fact, the design of the balance was performed based on the Apollo’s aerodynamic coefficients at trim angle, whereas the H3 limitations (e.g., blockage) did not allow to successfully test beyond the limit AoA of 4° during the preliminary tests for the definition of the official testing configuration. Consequently, although the axial force appeared to be within the design range thanks to its small dependence on the AoA, the measured normal force and the pitching moment fell significantly below the nominal design point. However, analyzing the recorded voltage for the cases at 0° AoA and comparing with the balance calibration data, it appears that there is an order of magnitude difference between the actual measured values of F_z and M_y and those that could be expected if only a cross-link effect (i.e., noise) were generating a voltage for these two components. Hence, it seems possible that a real normal force was acting on the models during these tests at 0° AoA. The most probable explanation for this would be a side effects such as the interaction between the model and its support and requires further investigations.

For what concerns the variation of the coefficients with the AoA, the analysis of the entry point reveals that the C_{F_x} is slightly affected by the AoA. This behavior seems reasonable and in line with literature data for other capsules (e.g., Apollo) considering the shape of the capsule and the small AoA variation analyzed. The situation is different for the C_{F_z} were a clear influence of the AoA is visible. As anticipated, the actual values of this coefficient may be affected by a side effect such as the influence of the model support, but the increase of the entry-point value with the AoA is evident and appears to be coherent with the expected behavior. The analysis of the entry values for the pitching moment C_{M_y} appears to be less obvious instead. The data at 0° AoA seems to be nicely clustered around the same value but this is not the case for the other AoAs. A detailed explanation for this trend would require further analysis.

It is important to mention that the data shown in Fig. 12 have been obtained without applying any correction to the measured data. However, the analysis of the recorded voltage right before injection and right after ejection

DOI: 10.13009/EUCASS2019-608

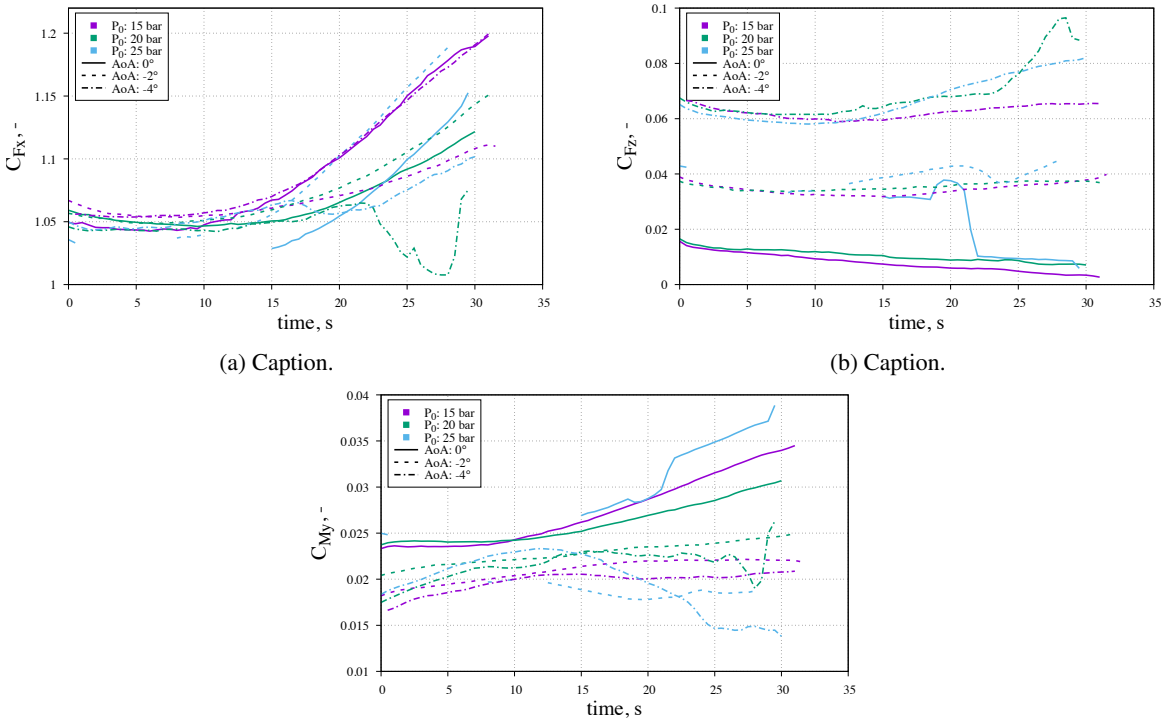

(a) Caption.

(b) Caption.

(c) A subfigure

Figure 12: Uncorrected aerodynamic coefficients for the whole test duration.

of the capsule in the testing position revealed that the measured normal force changed before and after the test. [1] This difference, partially expected due to the ablated mass, was further investigated using the data from the recession measurements that allowed to have an estimate of the mass loss of the capsule when axisymmetric ablation is assumed. This procedure was automated and implemented in the postprocessing tool to allow the correction of the excess of variation of the measured voltage that cannot be ascribed to the sole mass-loss effect and could be possibly caused by some sort of parasite effect on the balance (e.g., temperature effect). Due to the lack of additional data, this excess voltage was considered to increase linearly during the test from 0 at the injection time to the measured value at the ejection time, and was deducted from the measured data. Overall this correction did not change the qualitative behavior of the aerodynamic coefficients shown in Fig. 12 except for an accentuation of the small drop of C_{F_x} (for all AoAs) and C_{F_z} (for AoA $\neq$ 0) at the beginning of the test. However, if the variation of the capsule radius is taken into account in the evaluation of the coefficients, which is possible thanks to the on-side recession measurements that give an indication of the radius variation over time, the drop is significantly reduced. The corrected (for the parasite-effect drift and radius variation), normalized values of the coefficients are those given in Fig. 13 for the relevant time of the test (i.e., before the first of the failure mode given in Table 2 appears) as a function of the center-line recession. The axial-force coefficient, whose dimensional value is similar for all the test (see Fig. 12a), has a clearly increasing trend regardless the AoA or the total pressure. All the data, with the exception of test no. 8, seems to approach a similar slope for the non-dimensional variation of the coefficient in function of the centerline recession. The analysis appears to be less obvious for the other two coefficients. Indeed, any small imperfection in the quality of the heat shield (in particular at the region of the shoulder which is not easy to manufacture) would have a more significant impact on the normal force and on the pitching moment than on the axial force. Hence, the measurement of these coefficients is definitely more challenging. A general observation is that the slope of these coefficients is reversed during the test (only visible for the tests whose relevant test time is long enough), and this could be compatible with the exposure of the metal edge of the back shell to the flow. In fact, even though the “macroscopic" exposure of the metal edge is considered for the definition of the relevant test time in each test, it is believed that even an imperceptible exposure of this edge could have a visible impact on the test data. Analyzing the normal-force coefficients for tests no. 1 to 6, it appears that this inversion occurs for a recession value that decreases with the total pressure changing from 15 bar to 20

[1] The H3 injection mechanism translate the capsule in the horizontal direction and rotate it around its axis. Hence, since the balance components are nullified with the capsule in the testing position, the recorded normal force (projection of the weight on the rotated $z-$axis) is different than 0 when the capsule is in its stand-by position out of the jet.

DOI: 10.13009/EUCASS2019-608

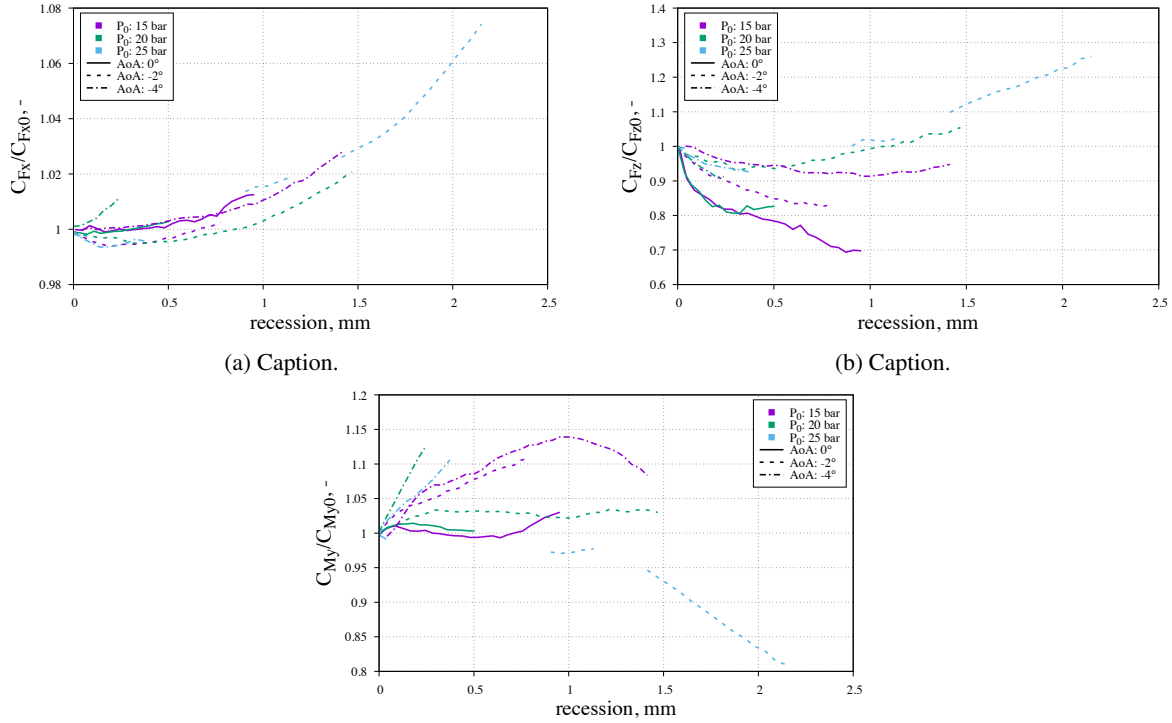

(a) Caption.

(b) Caption.

(c) A subfigure

Figure 13: Aerodynamic coefficients for the relevant test time plotted versus the center-line recession. Correction for the drift on the measurements and the crossflow are and radius have been applied.

bar. Unfortunately, the data at 25 bar are generally not satisfactory for the most of the cases and do not allow to verify this trend. The data for the tests at 15 bar, generally less problematic than the tests at higher pressures, suggests that the initial drop (possibly the real effect of the shape change before the heat shield deteriorates, for instance when the metal edge exposure kicks in) increases its slope with a decreasing AoA. However, it has to be noted that a quantitative comparison of the different curves is misleading since the normalization was performed using the entry value of each test. However, a similar observation cannot be made for the data at 20 bar as the values for the two higher AoAs are inverted. Finally, for what concerns the pitching moment, an increasing slope with the pressure is observed before the inversion. With the slope of the tests at 0° AoA close to 0.

7. Conclusions

We presented here a first analysis of the results of the tests performed on subscale ablative capsules in the VKI H3 hypersonic wind tunnel. The selection of the capsule shape (Phoebus) and the “surrogate" heat shield material (camphor) were performed based on a theoretical and numerical analyses that addressed the fact that a real ablator could not undergo relevant ablation in a low-enthalpy hypersonic wind tunnel. In particular, the analysis of the relevance of the behavior of the low-temperature heat shield with respect to the real-flight TPS is the main subject of parallel works[1] and has been discussed only briefly. A sintering procedure for the model manufacturing was developed and has been described. The advantages and disadvantages of using low-temperature ablators to manufacture the capsule’s heat shield with the conceived procedure have been also analyzed.

A complex measurement setup including optical measurements for recession and balance measurements for the forces was implemented for this test campaign. The performance of these measurement techniques has been discussed and the complexities added by the specific model setup (materials) and testing configuration have been detailed. Overall the measurement chain allowed to obtain relevant data and a first analysis of this measurement has been presented. This analysis focused on the description of the variation of the axial-force, normal-force, and pitching-moment of the capsule when the heat shield is subject to ablation and shape change. Indeed, a significant shape change was obtained during the test of the ablative subscale models, with a more important recession in the stagnation-point region than in the conical part of the heat shield. The heat-shield shoulder, which was the most difficult part to manufacture correctly, was also made of the low temperature ablator and appeared to be the most critical part for what concerns the effect

DOI: 10.13009/EUCASS2019-608

of the ablation on the aerodynamic coefficients. Indeed, an uneven recession of the heat shield in that region could affect significantly the normal force and the pitching moment. Moreover, a significant recession of the shoulder could lead to a direct exposure of the edge of the metal back shell of the capsule to the flow, with direct consequences on its aerodynamic behavior.

A detailed review of the test results obtained by testing a total of nine different conditions (three Angles of Attack (AoAs) and three different total pressures) is still ongoing, yet the analysis presented here has given some first indications about the possible influence of the heat-shield shape change on the aerodynamic coefficients. The analysis of the axial-force coefficients has revealed an increase of this quantity during the test. Indeed, the more pronounced recession of the stagnation point increases the capsule bluntness with time. The normal-force one, instead, shows a first drop followed by an increase that probably occurs when the shoulder recession is such that the metal edge of the back cover is exposed to the flow, as it seems to occur more clearly when an AoA is present. However, a non negligible value for this coefficient (with constant drop during the test in this case) has been observed also for the cases with 0° AoA, which suggests that some sort of side-effects related to the test setup could be influencing the aerodynamic behavior of the capsule. This point has yet to be fully understood and should be the subject of the next phase of the data analysis. The analysis of the pitching moment, after a series of corrections was applied to the raw balance data, has revealed that the relative increase of this quantity (with respect to the value measured as soon as the capsule is injected) is more significant for the high-pressure cases.

As anticipated , the analysis of the data is still in its first phase although few interesting behavior could already be detected. The ongoing analysis focuses on a more detailed review of the experimental data and will be the subject of future works.

8. Acknowledgments

This work was performed under the European Space Agency contract no. 4000121241/17/NL/KML: “Modelling Capsule Stability Accounting for Shape Change.” The paramount work of the H3 team, Patrick Danneels and Pascal Collin, in supporting the preparation of the tests and operating the facility is truly acknowledged, together with the fundamental work of Vincent Van der Haegen , the VKI Workshop, and the VKI Drawing Office in the design and manufacturing of the numerous hardware needed to perform this activity. A. Turchi would also like to sincerely thank his colleagues Dr. Davide Masutti, Dr. Damien Le Quang , and Dr . Bernd Helber for the numerous precious technical discussions on different related subjects and their practical help with the experimental setup.

References

[1] Daniele Bianchi and Alessandro Turchi. Numerical analysis on the sublimation of low-temperature ablators models undergoing shape change in a supersonic wind-tunnel. In *8th European Conference for Aeronautics and Aerospace Sciences (EUCASS)*, 2019.

[2] Andrew F. Charwat. The preparation of camphor models for windtunnel sublimation studies; preliminary results on the sublimation of a pointed cone. Technical report, Rand Corp. Santa Monica CA, 1962.

[3] Luca Ferracina, Lionel Marraffa, and Jose Longo. Phoebus: A hypervelocity entry demonstrator. In *ESA Special Publication*, volume 714, 2012.

[4] B. J. Griffith and D. E. Boylan. Reynolds and mach number simulation of apollo and gemini re-entry and comparison with flight. 1968. NASA Technical Report.

[5] Mark A. Havstad and Robert M. Ferencz. Comparison of surface chemical kinetic models for ablative reentry of graphite. *Journal of Thermophysics and Heat Transfer*, 16(4):508–515, 2002.

[6] Bernd Helber, Alessandro Turchi, and Thierry E Magin. Determination of active nitridation reaction efficiency of graphite in inductively coupled plasma flows. *Carbon*, 125:582–594, 2017.

[7] Bernd Helber, Alessandro Turchi, James B Scoggins, Annick Hubin, and Thierry E Magin. Experimental investigation of ablation and pyrolysis processes of carbon-phenolic ablators in atmospheric entry plasmas. *International Journal of Heat and Mass Transfer*, 100:810–824, 2016.

[8] Lester Lees. Laminar heat transfer over blunt-nosed bodies at hypersonic flight speeds. *Journal of Jet Propulsion*, 26(4):259–269, 1956.

DOI: 10.13009/EUCASS2019-608

[9] Stefan Loehle, Tina Staebler, and Thomas Reimer. Photogrammetric surface analysis of ablation processes in high enthalpy air plasma flow. In *11th AIAA/ASME Joint Thermophysics and Heat Transfer Conference*, page 2248, 2014.

[10] Stefan Löhle and Thomas Reimer. Experimental investigation of photogrammetric surface analysis of heat shield materials during plasma wind tunnel testing. In *7th ESA Thermal Protection Workshop*, 2013.

[11] Thomas Luhmann, Stuart Robson, Stephen Kyle, and Ian Harley. Close range photogrammetry: Principles. *Methods and Applications*, page 528, 2006.

[12] Megan E. MacDonald, Carolyn M. Jacobs, Christophe O. Laux, Fabian Zander, and Richard G. Morgan. Measurements of air plasma/ablator interactions in an inductively coupled plasma torch. *Journal of Thermophysics and Heat Transfer*, 29(1):12–23, 2014.

[13] Thomas Reimer, Stefan Löhle, and Rainer Öfele. Photogrammetric surface recession measurements on ablative samples of various shape. *Processing, Properties, and Design of Advanced Ceramics and Composites*, 259:373, 2016.

[14] Thomas Reimer, Rainer Öfele, and Stefan Löhle. Ablation recession measurements in arc jet tests via photogrammetric observation. In *8th European Workshop on Thermal Protection and Hot Structures*, 2016.

[15] Edward T. Schairer and James T. Heineck. Photogrammetric recession measurements of ablative materials in arcjets. *Measurement Science and Technology*, 21(2):025304, 2010.

[16] Hans W. Stock and Jean J. Ginoux. Hypersonic low temperature ablation an experimental study of cross-hatched surface patterns. In *VKI Technical Note 64*. von Karrman Institute, 1971.